ARCHIVES OF CIVIL AND MECHANICAL ENGINEERING 15 (2015) 836–846

Available online at www.sciencedirect.com

ScienceDirect

journal homepage: http://www.elsevier.com/locate/acme

Original Research Article

Constitutive modelling effect on the numerical prediction of springback due to a stretch-bending test applied on titanium T40 alloy

A. Maati [a,b,*], L. Tabourot [c], P. Balland [c], E.H. Ouakdi [a], M. Vautrot [c], N. Ksiksi [c]

[a] Laboratoire de Physique et Mécanique des Matériaux Métalliques, Institut d'Optique et Mécanique de Précision, Université Ferhat Abbas Sétif 1, 19000, Algeria

[b] Laboratoire de Génie des Procédés, Université Amar Telidji de Laghouat, 03000, Algeria

[c] Laboratoire SYMME, Université de Savoie, 74944 Annecy-le-Vieux, France

ARTICLE INFO

Article history:
Received 19 November 2014
Accepted 26 May 2015
Available online 3 July 2015

Keywords:
Springback
Hybrid model
Kinematic hardening
Anisotropy
Stretch-bending

ABSTRACT

Nowadays, numerical simulation by finite element analysis is an essential tool that allows performing virtually sheet metal forming processes, and therefore to reproduce various phenomena such as springback (SB) and necking that are generated by plastic deformation. However, the quality of the model used to represent the mechanical behaviour is a determining factor for the realism of numerical simulations. To perform well, the model must reproduce all the properties of the material such as the anisotropy and the strain hardening induced by plastic deformation. The main purpose of this work is to show, by means of numerical simulations, the influence of constitutive modelling on the prediction of the degree of SB in the case of a stretch bending test. Tests have been carried out on titanium sheets which have a wide range of applications for high tech industries because of specific mechanical and physical properties. At the same time, we have investigated the dependence of some process parameters such as the clamping force on SB. In order to prove the accuracy and reliability of the proposed finite element model, experimental data were used to compare with the numerical results.

1. Introduction

After the sheet metal forming operation, SB due to the elastic material behaviour can lead to shape errors that cause geometrical and dimensional inaccuracies in the sheet metal forming processes, especially in bending operations [1]. The major cause that leads to and influences the instability phenomenon is the state of stress generated by the forming process in the material [2]. Therefore, it is very important to establish an interaction between SB and the distribution of stress through material behaviour law. The amount of SB is certainly affected by the material properties (such as Young's modulus, initial yield stress, Poisson's coefficient, strain

* *Corresponding author at*: LPMMM, IOMP, Sétif 1 University, 19000, Algeria. Tel.: +213 36 92 51 38; fax: +213 036 92 84 18.
E-mail address: a.maati@lagh-univ.dz (A. Maati).

http://dx.doi.org/10.1016/j.acme.2015.05.009

hardening exponent, etc.), the punch and die profile radii, the clearance between punch and die, the friction conditions, the blank holder force, etc. [3].

SB is known to be more severe for lightweight materials such as aluminium and titanium alloys due to the higher ratio of yield stress relative to elastic modulus [4]. Several studies have been done to show the influence of mechanical properties and technological factors on the amount of *SB* after forming process. Using numerical simulations, Xia et al. [5] have shown that the mechanical properties and the strain hardening law have an obvious effect on the accuracy of *SB* prediction. Ouakdi et al. [6] revealed through U-form stretch-bending tests on aluminium alloy that the *SB* decreases non-linearly with the stretching depth and that an increase in the clamping force reduces the sliding of the sheet between the die and the blank holder (*BH*) relatively.

The anisotropy effect due to the cold rolling process is also a major plasticity factor often introduced in some numerical models to predict *SB*. Verma et al. [7] showed that *SB* is greater if the sheet is bent perpendicularly to the rolling direction (*RD*). Hence *SB* depends strongly on the anisotropy ratio *r*.

Most works in the field make use of classic phenomenological models to describe the material's behaviour; these types of models being based upon simplifications of material description, which is very restrictive. Indeed, metallic materials often behave in complicated way, especially due to the heterogeneities of structure. Recently, a series of works [8–10] has been performed to highlight the influence of these heterogeneities on the plastic behaviour, kinematic hardening, anisotropy and the elastic behaviour. Models that take the local heterogeneities of material into account have been developed to forecast the *SB* or all other physical phenomena efficiency depending on the microscopic heterogeneities. In this category, Tabourot et al. [11] have proposed a hybrid model to investigate the localization phenomenon in the case of a tensile test on C68 grade steel. The model takes into account the physical phenomena at the microscopic level and especially the heterogeneities of material.

This paper is mainly devoted to the influence of these local heterogeneities on the numerical prediction of SB using case studies (stretch-bending tests). Titanium T40 was chosen as the material to be studied on the basis that the *SB* prediction is very difficult due to the structural heterogeneity of this material. In addition, the sheets of titanium are increasingly used in aircraft construction for making different parts because of its corrosion-resistivity and specific mechanical properties.

2. Material property calibration

2.1. *Experimental characterization*

A ductile alloy of great industrial importance was chosen for this study. The titanium T40 grade 2 is considered as an important alloy used in aerospace sheet metal products. In order to characterize the mechanical behaviour, a series of tensile tests was carried out at room temperature on flat samples with the geometry shown in Fig. 1. The tension test is carried out using displacement speed of 10 mm/min. In order

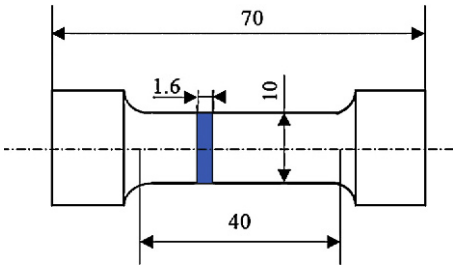

Fig. 1 – Shape and dimensions of the tensile test specimen.

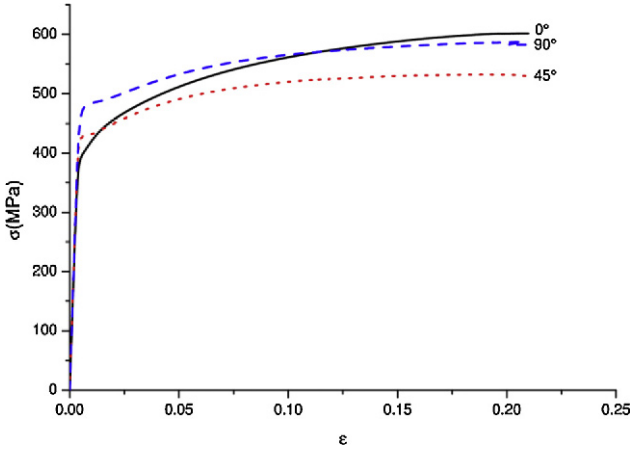

Fig. 2 – Cauchy stress vs. logarithmic strain for three titanium specimens cut at 0°, 45° and 90° relative to RD.

to take the anisotropy effect due to the cold rolling process into account, the material characterization must be performed at 0°, 45° and 90° with respect to RD. The deformations of the samples are measured using an image analysis method [12]. The true stress–strain curves of T40 alloy subjected to monotonic loading are given in Fig. 2.

The effect of normal anisotropy on the assessment of *SB* is considered in this work. In the literature, various models are proposed to describe anisotropic yielding of metals. Hill's quadratic yield criterion [13] is used for the current study. The advantage of this criterion is that it is available in the ABAQUS database. Analytically, Hill's quadratic yield function can be written as following:

$$2f(\sigma_{ij}) = \sqrt{\begin{matrix} F(\sigma_{22}-\sigma_{33})^2 + G(\sigma_{33}-\sigma_{11})^2 \\ +H(\sigma_{11}-\sigma_{22})^2 + 2L\sigma_{23}^2 + 2N\sigma_{12}^2 \end{matrix}} = 1 \quad (1)$$

where *F*, *G*, *H*, *L*, *M* and *N* are the material parameters characterizing the anisotropy effect.

In the case of thin metal sheets from which the assumption of plane stress can be made, this criterion amounts to an expression having only 4 parameters *F*, *G*, *H* and *N* since $\sigma_{i3} = 0$.

$$2f(\sigma_{ij}) = \sqrt{(G+H)\sigma_{11}^2 - 2H\sigma_{11}\sigma_{22} + (F+H)\sigma_{22}^2 + 2N\sigma_{12}^2} = 1 \quad (2)$$

In this work, the experimental values of Hill48 criterion parameters obtained by Toussaint et al. [14] were adopted ($F = 0.52$; $G = 0.29$; $H = 1.71$ and $N = 4.2$).

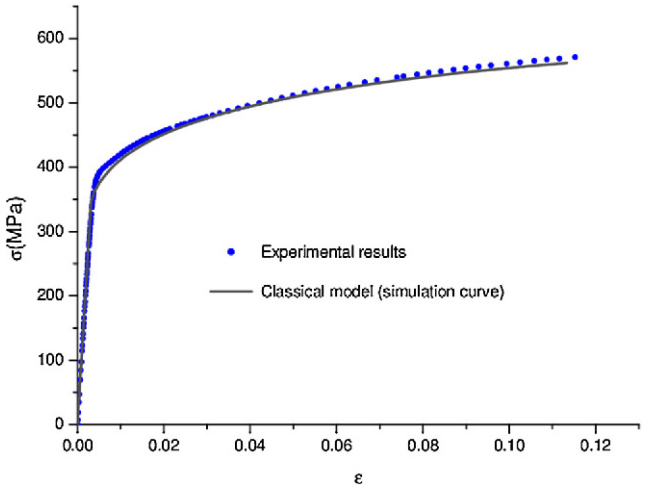

Fig. 3 – Experimental and numerical true stress-strain curves obtained for T40 alloy at constant crosshead speed (V = 10 mm/min).

2.2. *Presentation of the classic phenomenological model (CPM)*

At low strains, the material has linear, isotropic, elastic behaviour that is modelled by Hooke's law. The reference curve of its plastic behaviour can be adjusted to a numerical curve that follows Hollomon's power law given by:

$$\sigma = \sigma_y(\varepsilon_p)^N \tag{3}$$

σ_y and N represent the *CPM* parameters.

A Python programme was developed used to identify the constitutive model parameters. For instance, in the direction 0° (*RD*) the values σ_y = 350 MPa and N = 0.13 enable us to have a simulated curve that is very close to the experimental curve, as shown in Fig. 3. However, in order to have the precise reference curve that will be used as input data in the finite element code; the plastic strain is expressed as:

$$\varepsilon_p = \begin{cases} 0 & \text{if } \sigma \le \sigma_0 \\ \varepsilon - \dfrac{\sigma}{E} & \text{if } \sigma > \sigma_0 \end{cases} \tag{4}$$

σ_0 is the initial yield stress.

The assumption of homogeneous strain justifies the symmetry of stress and strain from the centre of the specimen. For instance, in accordance with the study conducted by Tabourot et al. [11], a tension test simulation with *CPM* was carried out on titanium T40 to confirm that the necking is located at the centre of the sample. A snapshot of the model is shown in Fig. 4.

2.3. *Presentation of the hybrid model (HM)*

Compared to a *CPM* usually reduced by simplifying assumptions, the *HM* can be more consistent so as to obtain a better description of the various phenomena, such as necking and *SB* generated by the sheet metal forming process. The hardening model takes into account the physical phenomena at the microscopic level and especially the heterogeneities of the material. On a more macro level, the proposed model allows an alternative approach that makes the combination between rheological models and finite element analysis method possible. The basic idea is therefore to assimilate a restricted rheological model for each mesh element of the structure.

2.3.1. *Description of the HM*

The hybrid model developed at the Symme laboratory is an extension at higher scale of a local model developed by Déprés et al. [15] for intragranular behaviour. It has somehow some similarities with the heterogeneous finite element approach proposed by Furushima et al. based on grain size distribution [16].

In this study, the local behaviour is modelled using an elastoplastic constitutive law with bilinear strain hardening.

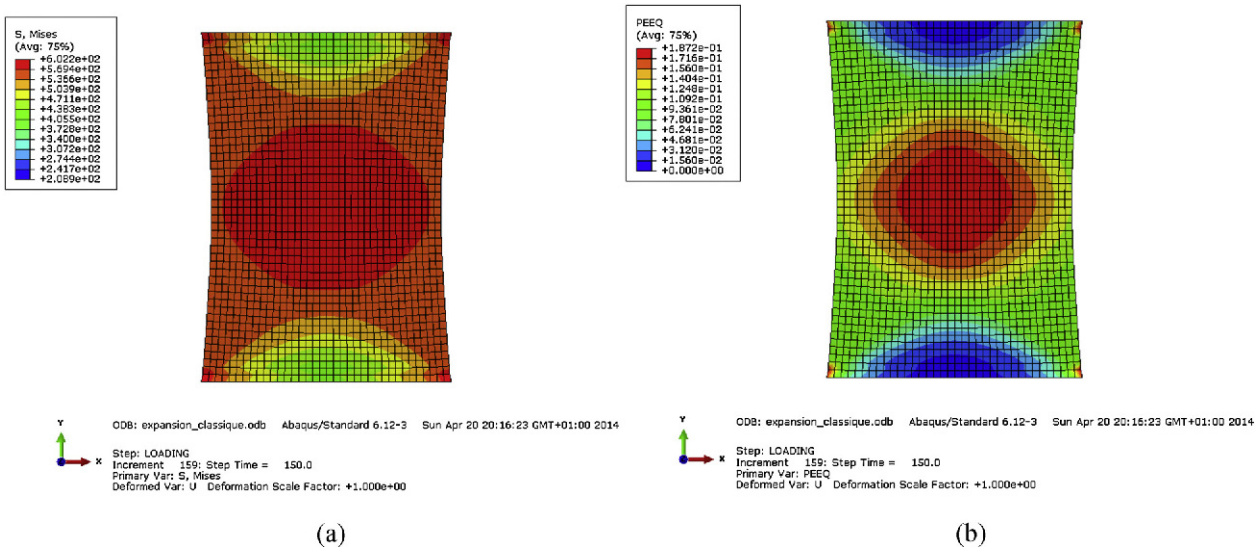

Fig. 4 – Symmetry of stresses and strains from the centre of the specimen during tensile test simulation using *CPM* (a) Von Mises stress (b) Equivalent strain.

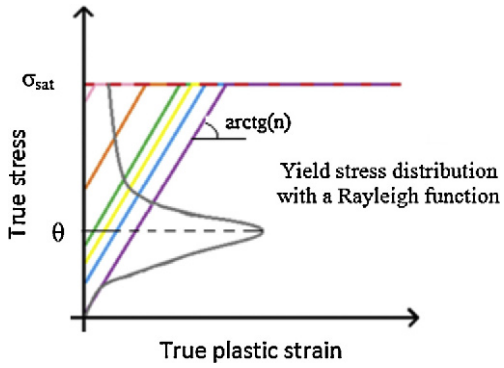

Fig. 5 – Local bilinear stress–strain hardening behaviour distribution [9].

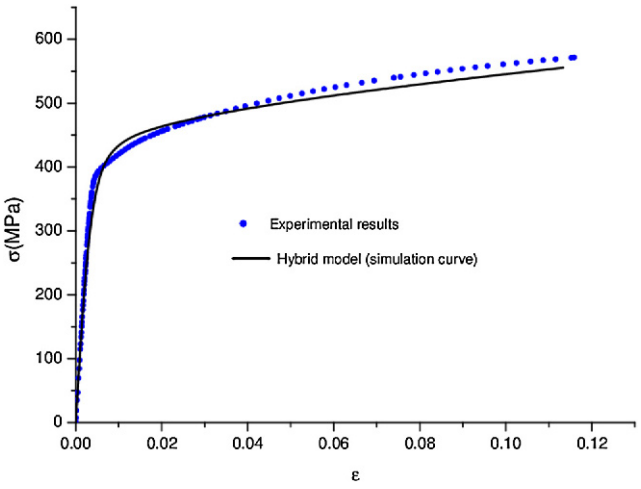

Fig. 6 – Experimental and numerical true stress-strain curves obtained for T40 alloy at constant crosshead speed (V = 10 mm/min).

The initial yield stress is distributed according to a Rayleigh's distribution which has the following mathematical form:

$$f\left(\frac{x}{\theta}\right) = \frac{x}{\theta^2} e^{\frac{-x^2}{2\theta^2}} \tag{5}$$

θ is an adjustable parameter which controls both the average and the standard deviation of the distribution and x is the variable which varies from 0 to infinity to define the distribution.

In Fig. 5, Rayleigh's distribution and the reference stress–strain curves describing the bilinear hardening distributed in each integration point of the elements of the mesh are presented.

The parameters of initial stress distribution are the average initial threshold stress θ, the saturation stress σ_{sat} and finally the slope n that defines the evolution of strain hardening. A Python script is used to identify the constitutive model parameters. The true stress–strain curve obtained numerically by the approximated values $\theta = 500$ MPa, $n = 575$ MPa and $\sigma_{sat} = 1346$ MPa shows good agreement with the experimental data as shown in Fig. 6.

Since it involves the material heterogeneities, the application of a *HM* reveals that, on the one hand, the necking does not necessarily occur in the middle of the sample but at any location in the useful area as shown in Fig. 7 and on the other hand, the kinematic hardening effect due to cyclic loading (tension-compression for example) can obviously be reproduced using this application, i.e. during a tension-compression cycle, yield stress at reload is higher than at the end of the first loading (Bauschinger effect) as shown in Fig. 8. RF2 and U2 represent the numerical force and the numerical displacement of the punch in Y direction respectively.

Consequently, taking into account the material heterogeneities in the constitutive model for predicting complex deformation history reduces the number of experimental tests required for the material characterization. For instance, the Bauschinger effect due to cyclic loading is

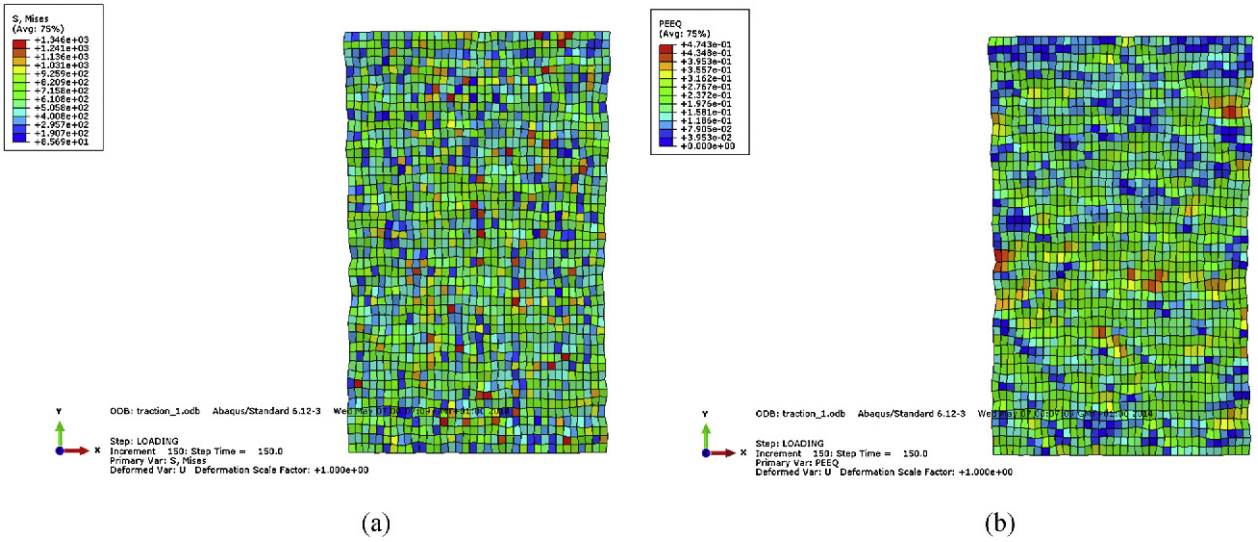

Fig. 7 – Numerical geometry of the sample after necking (strain map) simulated with the *HM*. (a) Von Mises stress. (b) Equivalent strain.

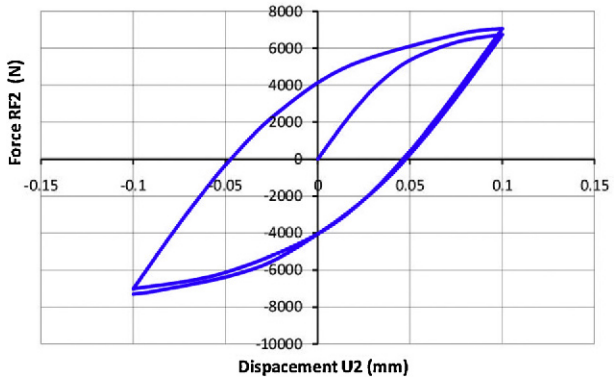

Fig. 8 – Bauschinger effect for T40 alloy reproduced during a tension-compression test simulation by applying a *HM*.

numerically reproduced without characterizing the kinematic hardening rule. The development of a routine that distributes properties over the elements of the mesh is the only extra work to do.

For comparison purposes between both forms of constitutive modelling, it is important to show the changes in the true stress–true strain for each referenced element (or node) during tensile test simulation. For this purpose, a loading path is chosen in the midline of the specimen marked in Fig. 9. Through *CPM*, it was observed that the true stress gradually increases along the loading path and reaches its maximum value at the centre of the specimen (node 9565) as shown in Fig. 10(a). Contrary to the previous simulation, the use of *HM* shows that the true stress varies randomly along the loading path and reaches its maximum value at any point of the specimen, as shown in Fig. 10(b).

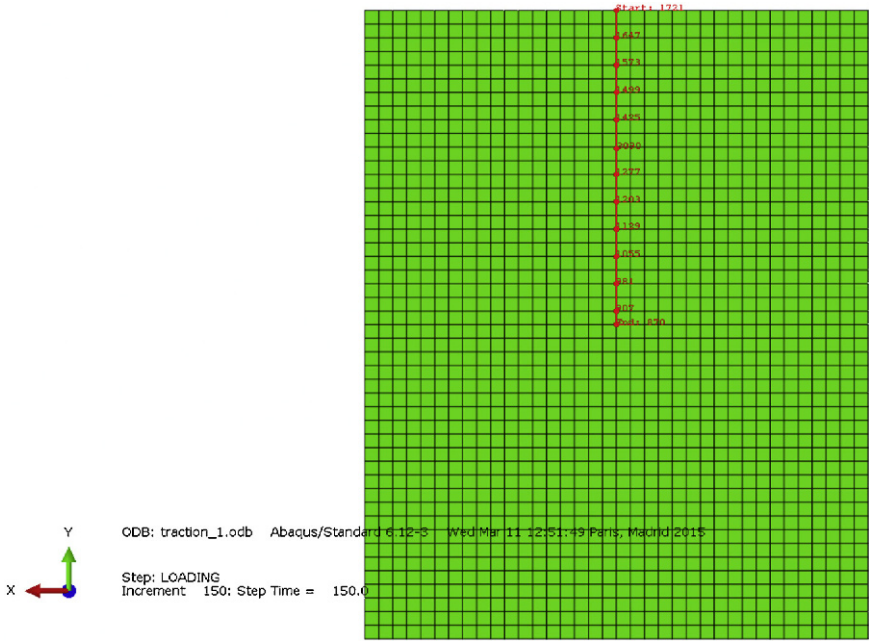

Fig. 9 – Loading path marked in the midline of the specimen.

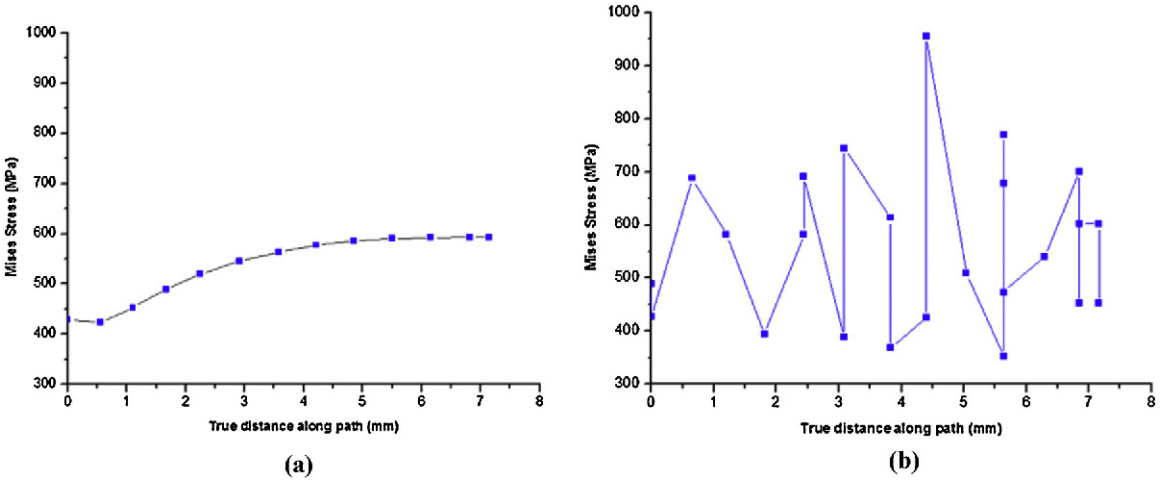

Fig. 10 – Evolution of the true stress along the loading path during tensile test simulation (for an imposed displacement $\Delta x = 1.5$ mm), (a) *CPM* case, (b) *HM* case.

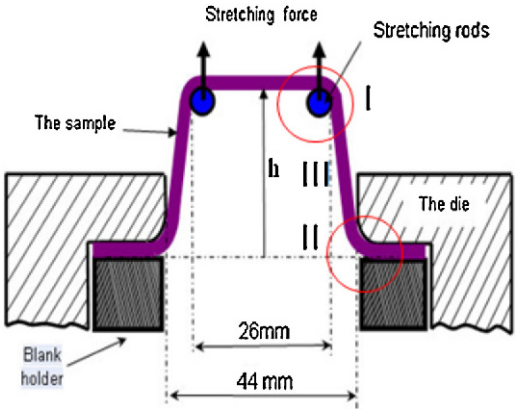

Fig. 11 – Principle of the stretch-bending process.

3. Numerical simulation of springback

3.1. *Presentation of the validation test*

The stretch-bending test that combines tension and flexion is the validation test used in this investigation to study the SB phenomenon. The principle of the current test is shown in Fig. 11.

Experimentally, this apparatus can be mounted on a tensile testing machine and gives one the possibility to vary several parameters. The die can be fixed on the mobile crosspiece of the tensile machine. The upper stretching piece is attached to the fixed crossbar of the tensile machine. As shown in Fig. 11, two parallel cylindrical rods act as the punch having a radius of curvature equal to $r_p = 4$ mm.

One of the advantages of this test is that it presents two dissimilar plies; first, V-bending may occur in two zones (I and II). The second, due to the sliding of the plate relative to the rod, is in fact a bending-unbending operation (zone III).

The stretch-bending test is governed by a set of parameters which have a significant impact on the final geometry of the formed product such as: clamping force CF, stretching depth h, die radius r_d, etc. The investigation of the influence of these parameters on SB is of paramount importance for the design and production of the tools.

Various tests were carried out to highlight the ''qualitative'' link that may exist between the parameters to be considered and the evolution of SB. These results served as an experimental baseline for the numerical simulations. The final geometry of the deformable specimen, after the removal of the tools, has two possible shapes as shown in Fig. 12 ($h2$ represents the stretching depth after freeing the test piece from the setup).

3.2. *Numerical simulation of a stretch-bending test applied to titanium T40 sheets*

This step aims to present a numerical simulation of a stretch-bending test that allows one to understand the SB characteristics of titanium sheet metals after discharge. Finite element

Table 1 – Material and geometrical data of the process elements.

Material of the blank	Characteristics of the blank					Tooling dimensions	Process parameters
Titanium T40 grade 2	Rectangular Plates Dimensions 126 × 10 × 1.6 (mm)					r_p = 4 mm	h = 12 mm
	E_{0° = 107,000 MPa					r_d = 5 mm	V = 3 mm/min
	E_{90° = 111,000 MPa					Clearance = 9 mm	S = 360 mm^2
	E_{45° = 113,000 MPa						CF = 0, 5, 13, 19 (KN)
	υ = 0.34						μ = 0.15
	Classical parameters		**0°**	**45°**	**90°**		
		N	0.13	0.11	0.09		
		σ_y (MPa)	350	355	420		
	Hybrid parameters		**0°**	**45°**	**90°**		
		θ (MPa)	500	500	549		
		n	575	480	436		
		σ_{sat} (MPa)	1346	1300	1434		

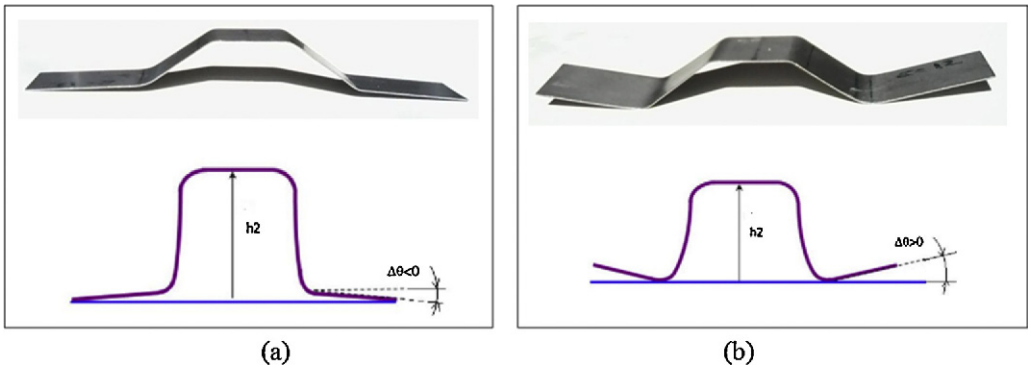

Fig. 12 – The two possible shapes of the deformable specimen after the removal of the tools.

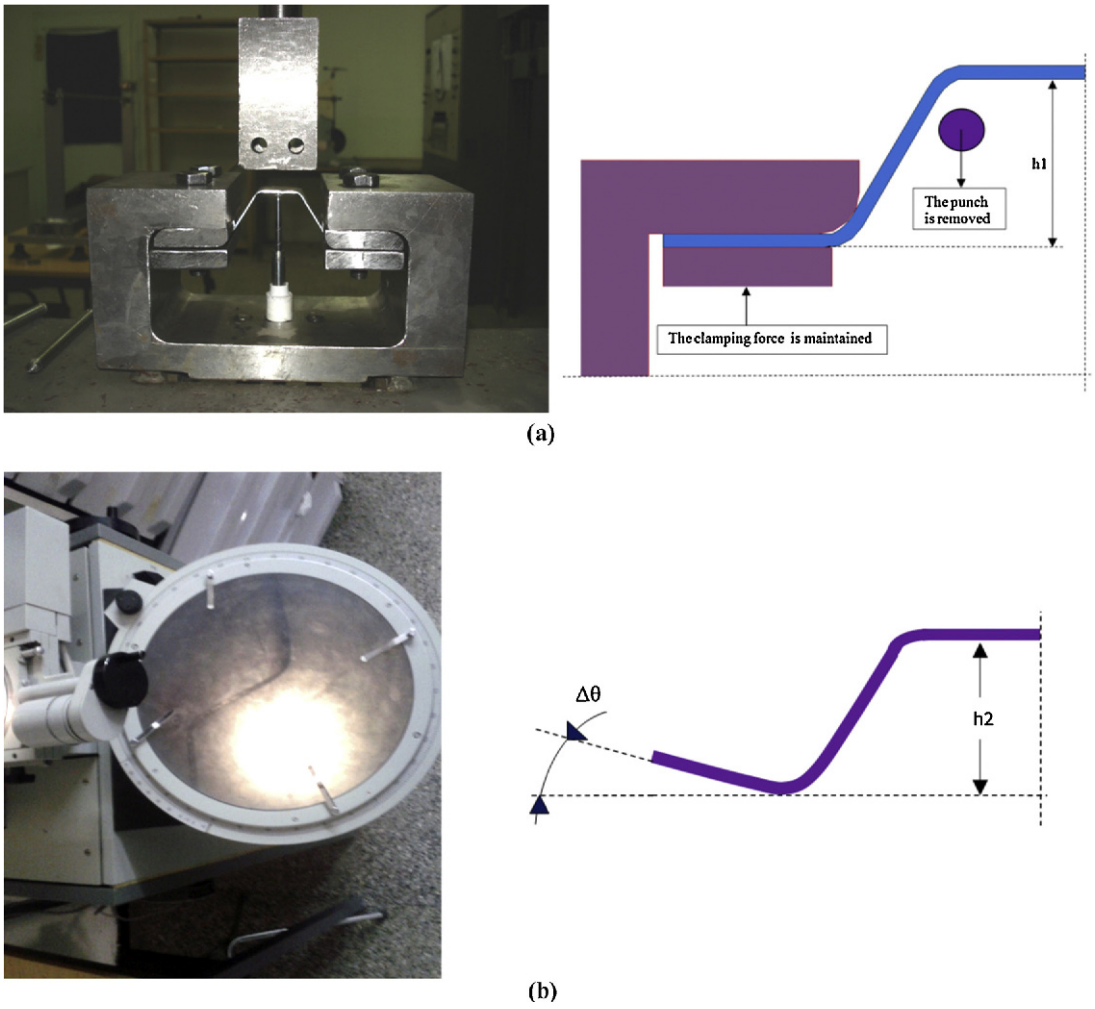

Fig. 13 – Geometric parameters of SB after: (a) removal of the punch only ($\Delta h1 = h - h1$); (b) freeing the test piece from the setup ($\Delta h2 = h - h2$), $\Delta\theta$ (or $h2$) was measured using profile measurer type MP320 (as shown in the picture).

analysis was carried out using Abaqus/standard software. The characteristics of the sheet, the dimensions of the tools and the process parameters are summarized in Table 1. The deformation of the test part was produced by an imposed displacement of the punch ($h = 12$ mm). In order to take into account the anisotropy effect in the numerical model, the Hill48 criterion was used. It was assumed that the elastic behaviour is described by a linear isotropic elastic law whose properties have already been determined by tensile experiments. The deformable part is meshed using C3D8R elements.

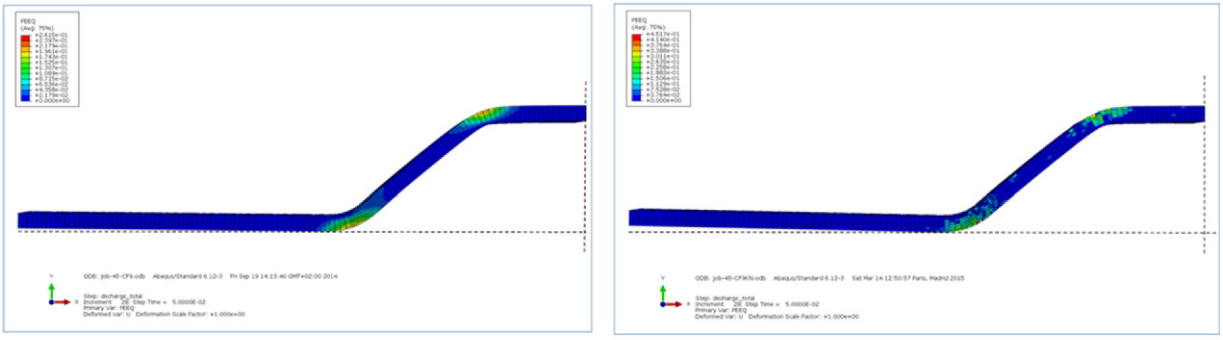

Fig. 14 – Example of the strain distribution in the sheet cut at 45° relative to RD and subjected to a clamping force equal to 9 KN, (a) and (b) represent the equivalent strain distribution through the thickness using *CPM* and *HM* respectively.

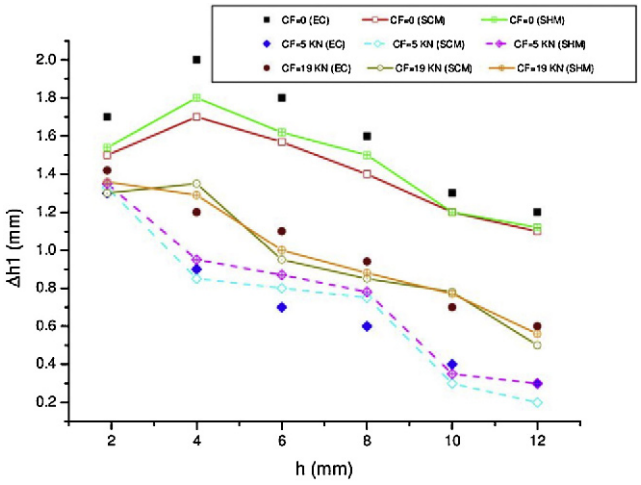

Fig. 15 – Δh1 changes with the increase of *h* for certain values of *CF* during stretch-bending tests (*EC*) Experimental curves; (*SCM*) Simulations with *CPM*; (*SHM*) Simulations with *HM*.

The die, the punch and the *BH* were assumed to be perfectly rigid. The clamping force is applied to the reference point of the *BH* in the form of concentrated force. *CF* on each end of the test piece is calculated from the tightening couple using the Kellermann–Klein formula [17], whereas the clamping pressure is calculated by dividing *CF* by the contact surface between the extremities of the test piece and the *BH* ($S = 360\ mm^2$). In order to take the different interactions between the rigid tools and the blank into account, a frictional coefficient ($\mu = 0.15$) was adopted to model the contact between the die and the blank surface as well as between the BH and the blank surface, whereas the friction effect between the punch and the blank was neglected. For reasons of symmetry, only one-quarter of the device need be modelled.

4. Results and discussion

4.1. *The influence of technological factors on* SB

Experimental and numerical studies were conducted to investigate the influence of certain significant parameters on *SB* amount. In order to clearly understand the combined

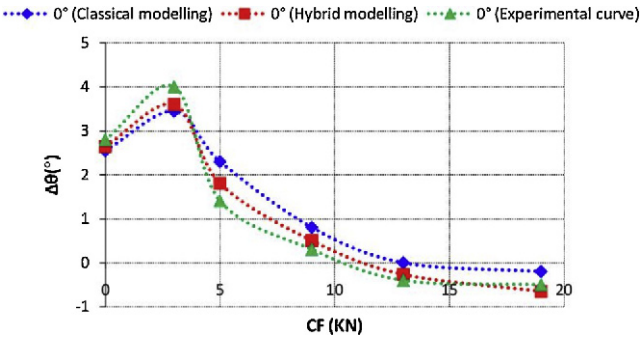

Fig. 16 – Prediction of final *SB* using the two proposed models (in the rolling direction).

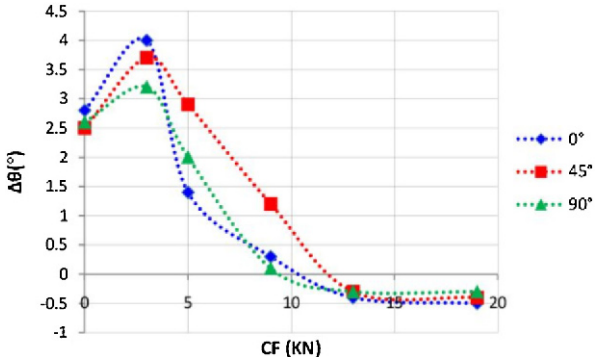

Fig. 17 – Experimental curves in three directions of sampling describing the relationship between the final *SB* and the clamping force for a given stretching depth (*h* = 12 mm).

effect resulting from the clamping force and the stretching depth on *SB*, several tests were carried out by varying these two parameters. As shown in Fig. 13(a), the primary *SB* $\Delta h1$ is calculated just after suppression of the stretching load from the difference between h and $h1$ (the clamping force is still maintained), whereas the final *SB* is evaluated using the geometric parameters $\Delta h2$ or else $\Delta\theta$ after the total release of the test part from the setup. $\Delta h2$ can be quantified linearly as the difference between h and $h2$, while $\Delta\theta$ is calculated by measuring the average angle between the ends of the test

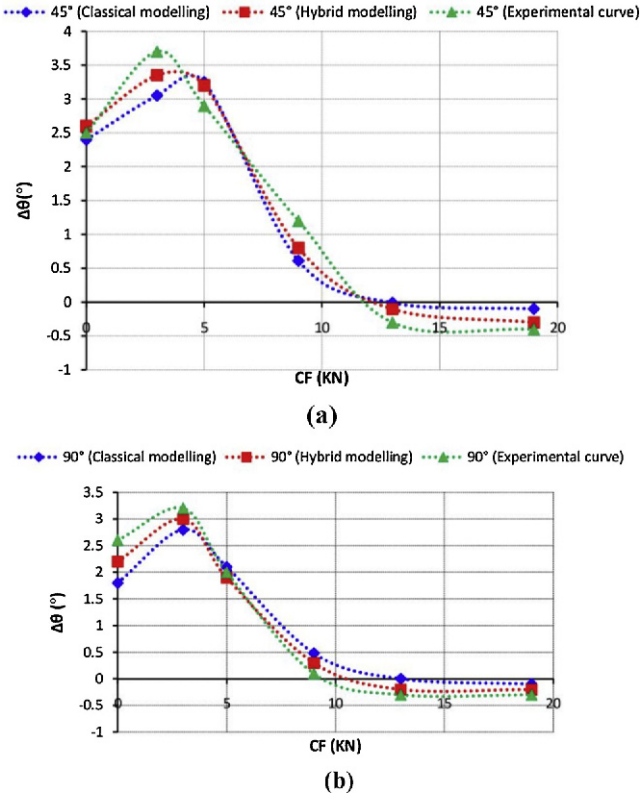

Fig. 18 – Anisotropy effect on final *SB* (a) Measurement performed in the direction 45° relative to *RD* (b) Measurement performed in the direction 90° relative to RD.

piece and the horizontal plane of the die. Experimentally, h is measured by the displacement captor and $h2$ (or else $\Delta\theta$) is measured by the profile measurer type MP320 having a precision of 0.001 mm (Fig. 13(b)). The final geometry of the deformable specimen depending on material behaviour modelling is illustrated in Fig. 14.

For comparison purposes (between both behaviour models), the internal distribution of strain was also illustrated in Fig. 14(a) and (b) for a case study (45°; h = 12 mm; CF = 9 KN).

In this study, the final SB has been measured via the angular amount $\Delta\theta$ typically simple compared to $\Delta h2$.

As shown in Fig. 15, it was observed that the effect of the clamping force on primary SB, $\Delta h1$, can be presented by two distinctive descriptions.

For a non-zero value of the clamping force, increasing h generates a gradual decrease of $\Delta h1$. The curve tends towards a steady state for a greater h (beyond h = 12 mm). In addition, the increase in the clamping force leads to a progressive increase in $\Delta h1$. This finding has been confirmed by some researchers in the field on steel and aluminium alloys [6,18]. This effect may be due to the higher plastic-hardening in the sheet metal induced concurrently by the high level of the clamping force and stretching depth.

For a clamping force equal to zero, the sheet slides smoothly between the die and BH. $\Delta h1$ is greater because of the very low stretching force in the sheet compared to the moment of bending which is very important in this case.

The final SB $\Delta\theta$ is determined after the test piece is completely removal from the machine. Using the two proposed models, $\Delta\theta$ decreases gradually with the increase in the clamping force as described in Fig. 16. It was found that the final SB becomes negative and takes the shape shown in Fig. 12(a) on reaching a certain value of the clamping force ($CF > 13$ KN in this case). This finding is the same as that reached by Ouakdi et al. [6]. The main difference between both models used in this study is the introduction of the heterogeneous distribution of mechanical properties. It is noticeable that a comparison of the results using numerical simulations shows that the error decreases if the constitutive law adopted for the material is finer, that is to say, it takes into account physical phenomena at the microscopic level, especially the heterogeneities of material.

4.2. *Anisotropy effect on* SB

In the case where the clamping force is lower ($0 \le CF < 3$ KN), as shown in Fig. 17, a large SB was observed for all three samples (0°, 45° and 90°) relative to RD. This increase is due to the effect of bending which dominates in the presence of significant sliding and weak stretching tension. For the large values of the clamping force (approximately $CF > 3$ KN), it has been noticed that the final SB decreases substantially towards a steady-state (generally negative). The final SB, expressed using the term $\Delta\theta$, continues to decrease negatively to reach

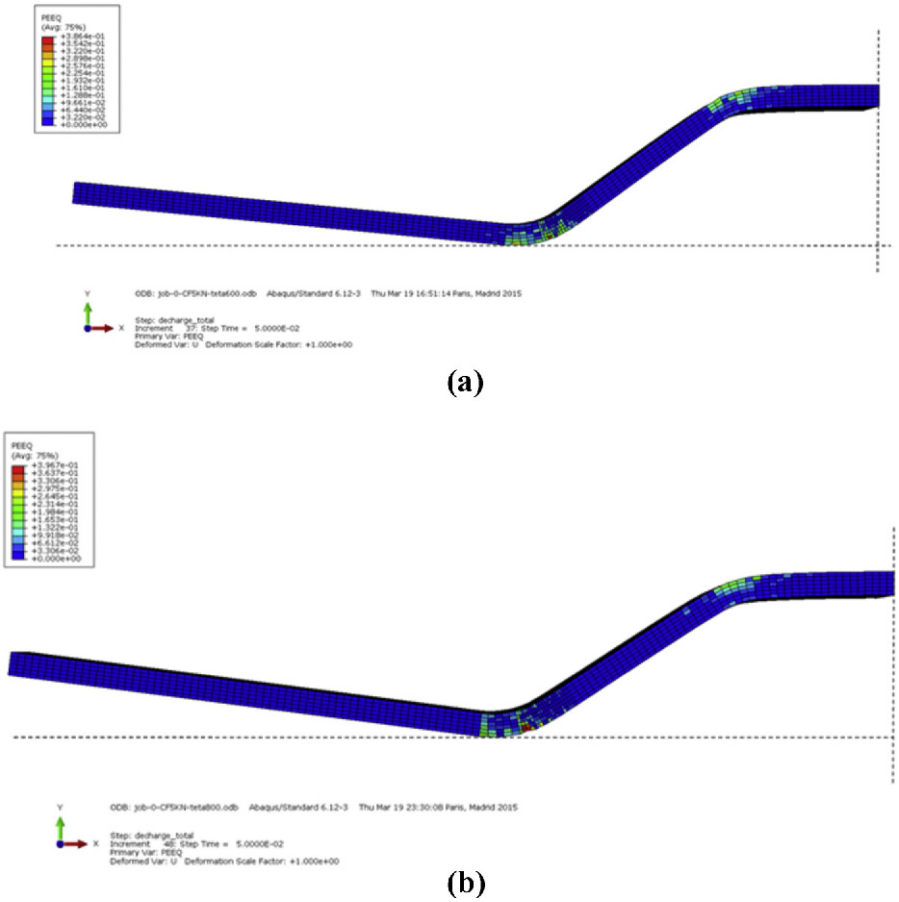

Fig. 19 – Effect of material heterogeneity on the springback, (a) h = 12 mm, CF = 5 KN, θ_1 = 600 MPa (b) h = 12 mm, CF = 5 KN, θ_2 = 800 MPa.

Table 2 – Value of SB at different levels of heterogeneity.

Distribution parameter θ (MPa)	500	600	700	800
Springback $\Delta\theta(^\circ)$	2	3.9	5.5	7.1

values slightly less than zero with the progressive increase of *CF*.

The effect of material anisotropy on the amount of *SB* is also predicted in the present work. The true stress-strain curve given in Fig. 2 for all three directions shows that, the selected alloy has less formability in the 45° direction compared to the 0° and 90° directions. For large plastic deformations ($\varepsilon_p > 10\%$), the same figure shows that the samples oriented in the directions 0° and 90° have very closely-related behaviour, therefore *SB* must be slightly different between the samples oriented in these directions.

In conclusion, as shown in Figs. 16 and 18(a) and (b), the experimental results and the numerical simulations that include two constitutive models of the material behaviour show that, for a small clamping force, the final *SB* is greater in the direction 0° compared to the other directions, whereas if the force increases to a certain level (3 KN < *CF* < 13 KN), it becomes more notable in the 45° direction. By increasing the force beyond the value *CF* = 13 KN, the final *SB* tends towards a steady-state value with a smaller difference between the sampling directions 0°, 45° and 90°. Below, the different graphs explicitly show the relationship between the final *SB* and the clamping force for a given stretching depth (h = 12 mm). Moreover, this geometrical change may be due to the variation of the mechanical characteristics of the specimen in the three directions such as Young's modulus and the hardening parameters.

A sensitivity analysis of *SB* to the random heterogeneous material was conducted. For this purpose, we have chosen four different levels of heterogeneity by increasing the distribution parameter θ of the hybrid model. In this paper, we treated one case corresponding to the boundary condition *CF* = 5 KN for a specimen cut in the rolling direction. It is concluded that the *SB* increases with the increase of the parameter θ characterizing the distribution of the local constitutive laws (Fig. 19). The results are summarized in Table 2.

5. Conclusion and perspective

In this paper, the following conclusions can be drawn:

- For zero clamping force, the *SB* is important because of the very low stretching force (even zero) applied to the sheet compared to the bending moment which is very important in this case.
- An increase in the amount of *CF* reduces the final *SB*. For the high values of CF (*CF* > 13 KN), it has been observed that *SB* is almost stable at a negative value $0 < \Delta\theta \leq -0.5^\circ$. This result is concordant with the results obtained by Ouakdi et al. [6].
- The tests on T40 titanium alloy reveal that *SB* depends closely on the material anisotropy. The final *SB* is greater in the direction 0° (*RD*) for a low value of clamping force. By increasing the value of *CF* up to 3 KN, *SB* increases noticeably in the 45° direction case compared to the other directions. By further increasing *CF* beyond the value *CF* = 13 KN, the final *SB* tends towards a steady state with a slight difference between the directions 0°, 45° and 90°.
- The primary *SB* $\Delta h1$ is not a decisive parameter to evaluate the effective *SB* in a final manufactured part, but it represents an important step in the numerical simulation process.
- Using *HM* can provide better results than those obtained by *CPM*; this is probably due to the fact that the *HM* takes into account the physical phenomena occurring during the plastic deformation of metallic materials; especially those related to the heterogeneities of internal material structure.
- The maximum difference between the numerical simulation and the experiment results expressed in relative error on final *SB* $(\Delta\theta_{exp} - \Delta\theta_{num})/\Delta\theta_{exp}$ is roughly 20% in the case of the application of the *HM*, whereas the error increases to around 30% for the *CPM*.
- Numerical simulations that integrate the *HM* have the advantage of being able to consider the kinematic hardening effect due to a cyclic loading induced by the bending-unbending of the sheet.
- Through this work, we have showed that T40 alloy undergoes large elastic recovery also due to its highly heterogeneous structure.

Finally, it can be concluded that the results generated by the numerical simulations of *SB* phenomenon are more accurate if the material heterogeneities are considered. These results also allow us to:

- accurately investigate the influence of other important factors on *SB* such as the radius of the curvature of the tool, stretching velocity, etc.
- use highly heterogeneous materials.

Acknowledgments

The present work was performed during several internships in Symme laboratory with financial support from Laghouat University.

REFERENCES

[1] H. Schilp, J. Suh, H. Hoffmann, Reduction of springback using simultaneous stretch-bending processes, International Journal of Material Forming 5 (2012) 175–180.
[2] N. Nanu, G. Brabie, Influence of material properties on the interaction between residual stress and springback in the case of in plane sheets forming, Archives of Civil and Mechanical Engineering XI (4) (2011) 979–990.
[3] A. Albut, G. Brabie, The influence of the rolling direction of the joined steel sheets on the springback intensity in the case of Ω-shape parts made from tailor welded strips, Archives of Civil and Mechanical Engineering VI (3) (2006) 5–12.
[4] F. Stachowicz, T. Trzepieciński, Warm forming of stainless steel sheet, Archives of Civil and Mechanical Engineering X (4) (2010) 85–94.

[5] C. Xia, C.E. Miller, F. Ren, Springback behavior of AA6111-T4 with split-ring test, in: Proceedings of the 8th International Conference on Numerical Methods in Industrial Forming Processes, NUMIFORM '04, 2004, 934–939.
[6] E.H. Ouakdi, R. Louahdi, D. Khirani, L. Tabourot, Evaluation of springback under the effect of holding force and die radius in a stretch bending test, Materials & Design 35 (2012) 106–112.
[7] R.K. Verma, A. Haldar, Effect of normal anisotropy on springback, Journal of Materials Processing Technology 190 (2007) 300–304.
[8] P. Balland, C. Déprés, R. Billard, L. Tabourot, Physically Based Kinematic Hardening Modelling of Single Crystal, American Institute of Physics, 2011, pp. 91–96.
[9] L. Tabourot, P. Balland, J. Raujol-Veillé, M. Vautrot, C. Déprés, F. Toussaint, Compartmentalized model for the mechanical behavior of Titanium, Key Engineering Materials 504–506 (2012) 673–678.
[10] L. Tabourot, P. Balland, M. Vautrot, O.S. Hopperstad, J. Raujol-Veillé, F. Toussaint, Characterization and modeling of the elastic behavior of a XC68 grade steel used at high strain rates and high temperatures, Key Engineering Materials 554 (2013) 1116–1124.
[11] L. Tabourot, P. Balland, N.A. Sène, M. Vautrot, N. Ksiksi, A. Maati, Numerical study of the impact of constitutive modelling on the evolution of necking in the case of a tensile test on C68 grade steel, Key Engineering Materials 611–612 (2014) 521–528.
[12] P. Vacher, S. Dumoulin, F. Morestin, S. Mguil-Touchal, Bidimensional strain measurement using digital images, Proceedings of the Institution of Mechanical Engineers 213 (1999) 811–817.
[13] R. Hill, A theory of the yielding and plastic flow of anisotropic metal, Proceedings of Royal Society of London A (193) (1948) 281–297.
[14] F. Toussaint, L. Tabourot, F. Ducher, Experimental and numerical analysis of the forming process of a CP titanium scoliotic instrumentation, Journal of Materials Processing Technology 19 (2008) 10–16.
[15] C. Déprés, M. Fivel, L. Tabourot, A dislocation-based model for low-amplitude fatigue behaviour of face-centred cubic single crystals, Scripta Materialia 58 (12) (2008) 1086–1089.
[16] T. Furushima, H. Tsunezaki, T. Nakayama, K. Manabe, S. Alexsandrov, Prediction of surface roughening and necking behavior for metal foils by inhomogeneous FE material modeling, Key Engineering Materials 554–557 (2013) 169–173.
[17] R. Kellermann, H.C. Klein, Studies of the Influence of Friction on Preload and Tightening Torque of Bolt Connections. Construction, vol. 2, Springer, 1955.
[18] K.P. Li, W.P. Carden, R.H. Wagoner, Simulation of springback, International Journal of Mechanical Sciences 44 (2002) 103–122.